Inorganica Chimica Acta 522 (2021) 120373

Contents lists available at ScienceDirect

Inorganica Chimica Acta

journal homepage: www.elsevier.com/locate/ica

Research paper

Azoimidazole gold(III) complexes: Synthesis, structural characterization and self-assembly in the solid state

Alexander G. Tskhovrebov [a,b,*], Alexander S. Novikov [c], Boris S. Tupertsev [a], Alexey A. Nazarov [d], Anastasia A. Antonets [d], Artyom A. Astafiev [a], Andreii S. Kritchenkov [b], Alexey S. Kubasov [e], Valentine G. Nenajdenko [d], Victor N. Khrustalev [b,f]

[a] N.N. Semenov Federal Research Center for Chemical Physics, Russian Academy of Sciences, Ul. Kosygina 4, Moscow, Russian Federation
[b] Peoples' Friendship University of Russia, 6 Miklukho-Maklaya Street, Moscow 117198, Russian Federation
[c] Saint Petersburg State University, Universitetskaya Nab. 7/9, 199034 Saint Petersburg, Russian Federation
[d] M. V. Lomonosov Moscow State University, Leninskie Gory 1, Moscow, Russian Federation
[e] Kurnakov Institute of General and Inorganic Chemistry, Russian Academy of Sciences, Leninsky Prosp. 31, Moscow, Russia Federation
[f] N. D. Zelinsky Institute of Organic Chemistry, Russian Academy of Sciences, 47 Leninsky Prosp, Moscow, Russian Federation

ARTICLE INFO

Keywords:
Gold(III)
Azoimidazoles
Heterocycles
Supramolecular polymers
Non-covalent interactions
Halogen-halogen interactions

ABSTRACT

Preparation of novel triarylazoimidazole trichlorogold(III) complexes is described. The new compounds were characterized using C, H, N elemental analyses, IR, UV/Vis and X-ray diffraction analysis. Structural characterization revealed that the distances N(imidazolic)···Au (2.030 Å (**4**) and 2.037 Å (**5**)) are significantly shorter than N(azo group)···Au (2.853 Å (**4**) and 2.899 Å (**5**)) indicating that the azo group is rather weakly coordinated at the Au(III) metal center. Thus, triarylazoimidazole trichlorogold(III) complexes could be described as square planar gold(III) complexes with weakly binding to the gold(III) center azogroup. Non-covalent chlorine···chlorine interactions were detected for **5** in the solid state and studied by DFT calculations and topological analysis of the electron density distribution within the framework of Bader's theory (QTAIM method). Theoretical studies demonstrated that short non-covalent Cl···Cl interactions (3.202 Å) play crucial role in self-assembly of high-valent Au(III) chloride.

1. Introduction

Azoimidazoles are important class of dyes, which are produced industrially and find broad applications for dying natural and synthetic fibers due to their easily tunable absorption properties [1]. Moreover, azoimidazoles, being a class of widely studied photoswitchable azo-compounds are attractive for applications in photopharmacology and bioinorganic chemistry since imidazole moiety is a ubiquitous and essential group in biology, often serving as a supporting ligand in metal-containing systems [2,3]. In the context photoactivated chemotherapy, photoswitchable late transition metal complexes hold promise for the development of novel methods which would feature advantageous control of drug-action specificity [4]. Therefore, exploration of coordination chemistry of cytotoxic metals, which contain potentially photoswitchable heterocyclic ligands seemed as an attractive niche.

Azoimidazoles have been intensively studied as ligands in coordination chemistry [5–9]. Currently, azoimidazole complexes are reported for many transition metals, while some of them exhibit intriguing photochromic properties [3,5,6]. In addition, they are attractive as chelating bidentate ligands, which electronic and photophysical properties could be easily tuned by substituents, which could be easily varied.

Surprisingly, azoimidazole-based gold(III) derivatives remained unexplored until now. Here we report a synthesis and characterization of first gold(III) azoimidazole complexes.

2. Experimental part

2.1. General remarks

Unless stated otherwise, all the reagents used in this study were obtained from the commercial sources (Aldrich, TCI-Europe, Strem, ABCR). The ligands **2** and **3** were synthesized according to the literature procedure, see Supporting Information [10]. NMR spectra were

* Corresponding author.
E-mail address: tskhovrebov-ag@rudn.ru (A.G. Tskhovrebov).

https://doi.org/10.1016/j.ica.2021.120373
Received 7 December 2020; Received in revised form 28 February 2021; Accepted 26 March 2021
Available online 30 March 2021

recorded on a Bruker Avance III (^{1}H: 400 MHz); chemical shifts (δ) are given in ppm relative to TMS, coupling constants (J) in Hz. The solvent signals were used as references ($CDCl_3$: $\delta_C = 77.16$ ppm; residual $CHCl_3$ in $CDCl_3$: $\delta_H = 7.26$ ppm; CD_2Cl_2: $\delta_C = 53.84$ ppm; residual $CHDCl_2$ in CD_2Cl_2: $\delta_H = 5.32$ ppm); ^{1}H and ^{13}C assignments were established using NOESY, HSQC and HMBC experiments; numbering schemes as shown in the Inserts. IR: Perkin-Elmer Spectrum One spectrometer, wavenumbers ($\tilde{\nu}$) in cm^{-1}. C, H, and N elemental analyses were carried out on a Euro EA 3028HT CHNS/O analyzer. Absorption spectra were measured in a 4 mL quartz cuvette using a UV–VIS spectrometer (UV-3600, Shimadzu). Solvents were purified by distillation over the indicated drying agents and were transferred under Ar: Et_2O (Mg/anthracene), CH_2Cl_2 (CaH_2), hexane (Na/K).

The MCF7, A549, HCT116 and WI38 cell lines were cultured in Dulbecco modified Eagle's medium (DMEM; Gibco, UK) with 10% fetal bovine serum (Gibco, USA) and antibiotics (PanEco, Russia) in 5% CO_2, 37 °C. The compounds were pre-dissolved at 20 mM in DMSO and added to the cell culture at the required concentration with maximum DMSO content of 0.5 v/v%. Cells in 96-well plates (7×10^3 cells/well) were treated with various concentrations of compounds and cisplatin at 37 °C for 72 h. Cell viability was determined using the MTT assay as follows: cells were incubated at 37 °C for 50 min with 100 μl of 5 mg/ml solution of 3-(4,5-dimethylthiazol-2-yl)-2,5diphenyltetrazolium bromide (Sigma-Aldrich, St. Louis, USA) in cell culture medium. The supernatant was discarded, and formazan was dissolved in 100 μl of DMSO. The optical density of the solution was measured at 570 nm on a multiwell plate reader (Multiskan FC, Thermo Fisher Scientifics, USA). The percentage of viable (i.e., MTT converting) cells was calculated from the absorbance of untreated cells (100%). Each experiment was repeated three times, each concentration was tested in three replicates.

The single point calculations based on the experimental X-ray geometry of **5** have been carried out at the DFT level of theory using the dispersion-corrected hybrid functional ωB97XD [11] with the help of Gaussian-09 [M. J. Frisch, et. al., in Gaussian 09, Revision C.01, Gaussian, Inc., Wallingford, CT, 2010.] program package. The Douglas–Kroll–Hess 2nd order scalar relativistic calculations requested relativistic core Hamiltonian were carried out using the DZP-DKH and TZP-DKH basis sets [12,13] for all atoms. The topological analysis of the electron density distribution with the help of the atoms in molecules (QTAIM) method developed by Bader, electron localization function (ELF) and reduced density gradient (RDG) analyses have been performed by using the Multiwfn program (version 3.7) [14]. The VMD program [15] was used for visualization of noncovalent interactions (NCI). The Cartesian atomic coordinates for model dimeric associate are presented in Supporting Information, Table S1. The Hirshfeld surface analysis has been performed by using the CrystalExplorer program (version 17.5) [16]. The normalized contact distances (d_{norm} [17]) based on Bondi's van der Waals radii [18] were mapped into the Hirshfeld surface.

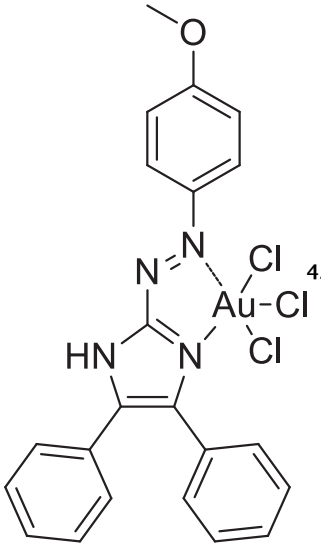

4. Azoimidazole **2** (0.118 mmol, 41 mg) was added to the solution of $NaAuCl_4$ $2H_2O$ (**1**) (0.118 mmol, 49 mg) in MeOH (1 mL). The resulting mixture was kept without stirring for 2 days; the formed precipitate was isolated by filtration, washed with MeOH (2 mL), Et_2O (3 × 2 mL), and dried under vacuum. Yield: 42 mg (53%). Elem. anal. calcd for $C_{22}H_{18}AuCl_3N_4O$·MeOH: C 40.05; H 3.21; N 8.12. Found: C 39.74; H 3.08; N 8.31. IR (ν): 1383 (NN), 1597 cm^{-1} (CN). UV/Vis (CH_2Cl_2): λ_{max} = 436 nm, $\varepsilon = 2.07 \times 10^4$ M^{-1} cm^{-1}. Crystals, suitable for X-ray analysis, were obtained directly from the reaction mixture.

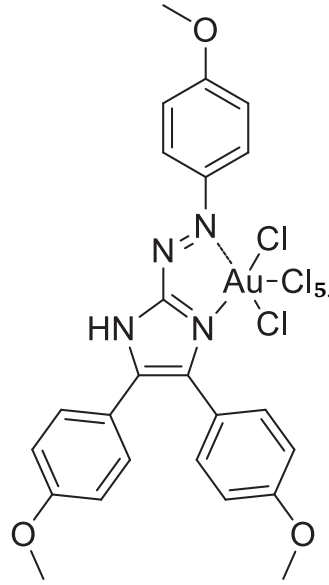

5. Azoimidazole **3** (0.126 mmol, 52 mg) was added to the solution of $NaAuCl_4$ $2H_2O$ (**1**) (0.126 mmol, 50 mg) in MeOH (1 mL). The resulting mixture was kept without stirring for 2 days; the formed precipitate was isolated by filtration, washed with MeOH (2 mL), Et_2O (3 × 2 mL), and dried under vacuum. Yield: 55 mg (61%). Elem. anal. calcd for $C_{24}H_{22}AuCl_3N_4O_3$·MeOH: C 40.05; H 3.50; N 7.47. Found: C 39.68; H 3.44; N 7.49. IR (ν): 1372 (NN), 1596 cm^{-1} (CN). UV/Vis (CH_2Cl_2): λ_{max} = 473 nm, $\varepsilon = 1.47 \times 10^4$ M^{-1} cm^{-1}. Crystals, suitable for X-ray analysis, were obtained directly from the reaction mixture.

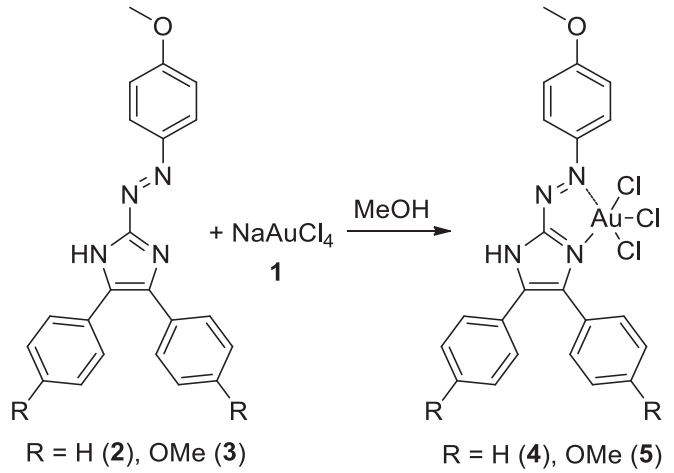

Scheme 1. Synthesis of diarylazoimidazole gold (III) complexes **4** and **5**.

3. Results and discussion

Gold(III) triarylazoimidazole complexes **4** and **5** were prepared in a moderate yield by the addition of corresponding triarylazoimidazole ligands **2** or **3** to $NaAuCl_4$ (**1**) in MeOH as a solvent (Scheme 1).

The structures and purity of new complexes were proved by C, H, N

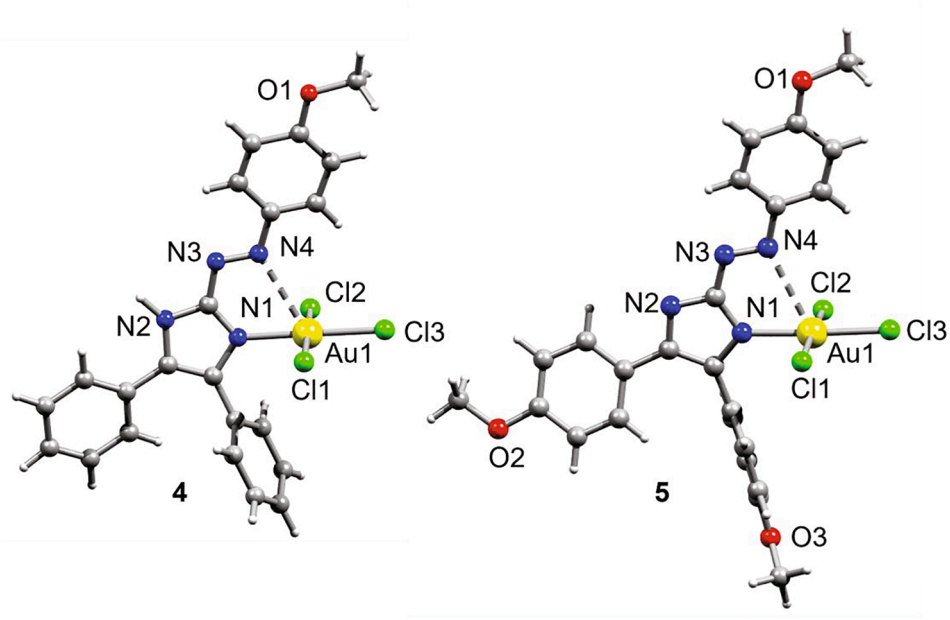

Fig. 1. Ball-and-stick representation of **4** and **5** in the crystal. Light-grey and grey spheres represent hydrogen and carbon atoms, respectively. MeOH molecules are omitted.

Table 1
Selected Bond Lengths (Å) and Angles (°) for **4**·MeOH and **5**·MeOH.

	4·MeOH	**5**·MeOH
Cl1–Au–Cl2	177.2(1)	175.4(8)
N–Au–Cl3	179.4(3)	177.4(1)
N–Au–N	64.5(3)	66.8(9)
Au–Cl1	2.289(4)	2.262(5)
Au–Cl2	2.267(4)	2.406(7)
Au–Cl3	2.252(4)	2.286(5)
Au–N1	2.030(9)	2.036(2)
Au–N4	2.853(1)	2.899(4)

elemental analyses, IR and X-ray diffraction analysis (Fig. 1, Table 1). Complexes **4** and **5** are very poorly soluble in common deuterated solvents, which precluded their analyses by the NMR in solution.

Compounds **4**·MeOH and **5**·MeOH precipitate from the reaction mixture as dark-red well-shaped blocks, suitable for analysis by single crystal X-ray crystallography. X-Ray analyses confirmed the formation of trichlorogold(III)-imidazole complexes for **4**·MeOH and **5**·MeOH (Fig. 1). Selected bond distances and angles for **4**·MeOH and **5**·MeOH are given in Table 1.

Overall, metrical parameters for organic ligands in **4**·MeOH and **5**·MeOH are similar to those reported for structurally relevant azo-compounds [1,19–22] and imidazole derivatives [23–26].

In both **4**·MeOH and **5**·MeOH the ligands form distorted square-based pyramid around the metal center with three chlorines and imidazolic N atom being nearly coplanar. The N atoms of the ligand adopt *cis* configuration around the metal center. Interestingly, the observed distances N1(imidazolic)···Au (2.030(9) Å (**4**·MeOH) and 2.036(2) Å (**5**·MeOH)) are significantly shorter than N4(azo group)···Au (2.853(1) Å (**4**·MeOH) and 2.899(4) Å (**5**·MeOH)) indicating that the azo group is rather weakly coordinated at the Au(III) metal center. Thus, the compounds **4** and **5** could be described as square planar gold(III) complexes

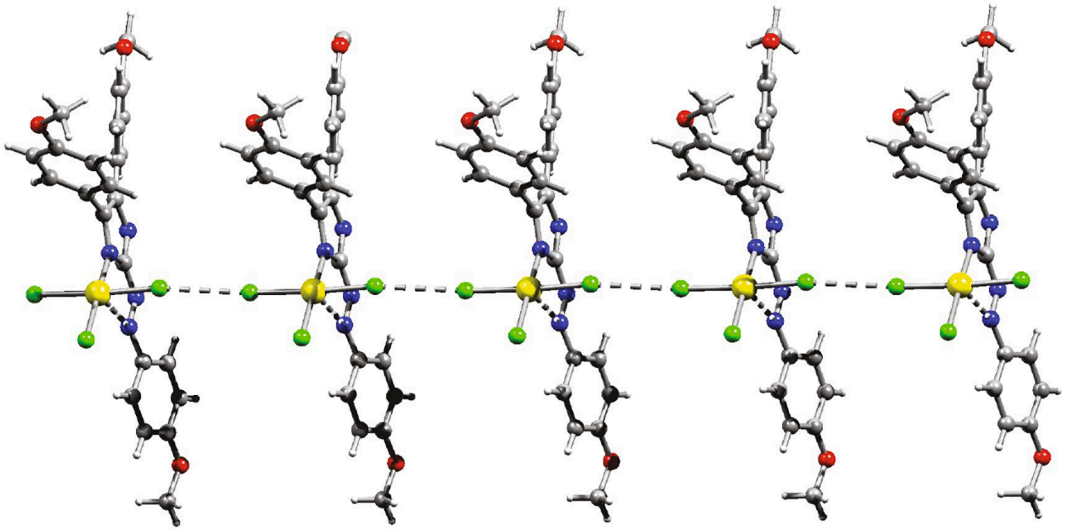

Fig. 2. Ball-and-stick representation of the structure of **5** in the crystal demonstrating its' self-assembly into infinite 1D chain *via* Cl···Cl non-covalent interactions. Yellow, blue, red, green, light-grey and grey spheres represent gold, nitrogen, oxygen, chlorine, hydrogen and carbon atoms, respectively.

Table 2
Values of the density of all electrons – ρ(**r**), Laplacian of electron density – $\nabla^2\rho(\mathbf{r})$ and appropriate λ_2 eigenvalue, energy density – H_b, potential energy density – V(**r**), and Lagrangian kinetic energy – G(**r**) (a.u.) at the bond critical point (3, –1) corresponding for Cl···Cl noncovalent interactions in **5** and their estimated strength E_{int} (kcal/mol).

Length of Cl···Cl contact is 3.202 Å *	ρ(**r**)	$\nabla^2\rho(\mathbf{r})$	λ_2	H_b	V(**r**)	G(**r**)	E^a_{int}	E^b_{int}
ωB97XD/DZP-DKH	0.010	0.040	–0.010	0.002	–0.006	0.008	1.8	2.4
ωB97XD/TZP-DKH	0.010	0.040	–0.010	0.002	–0.006	0.008	1.8	2.4

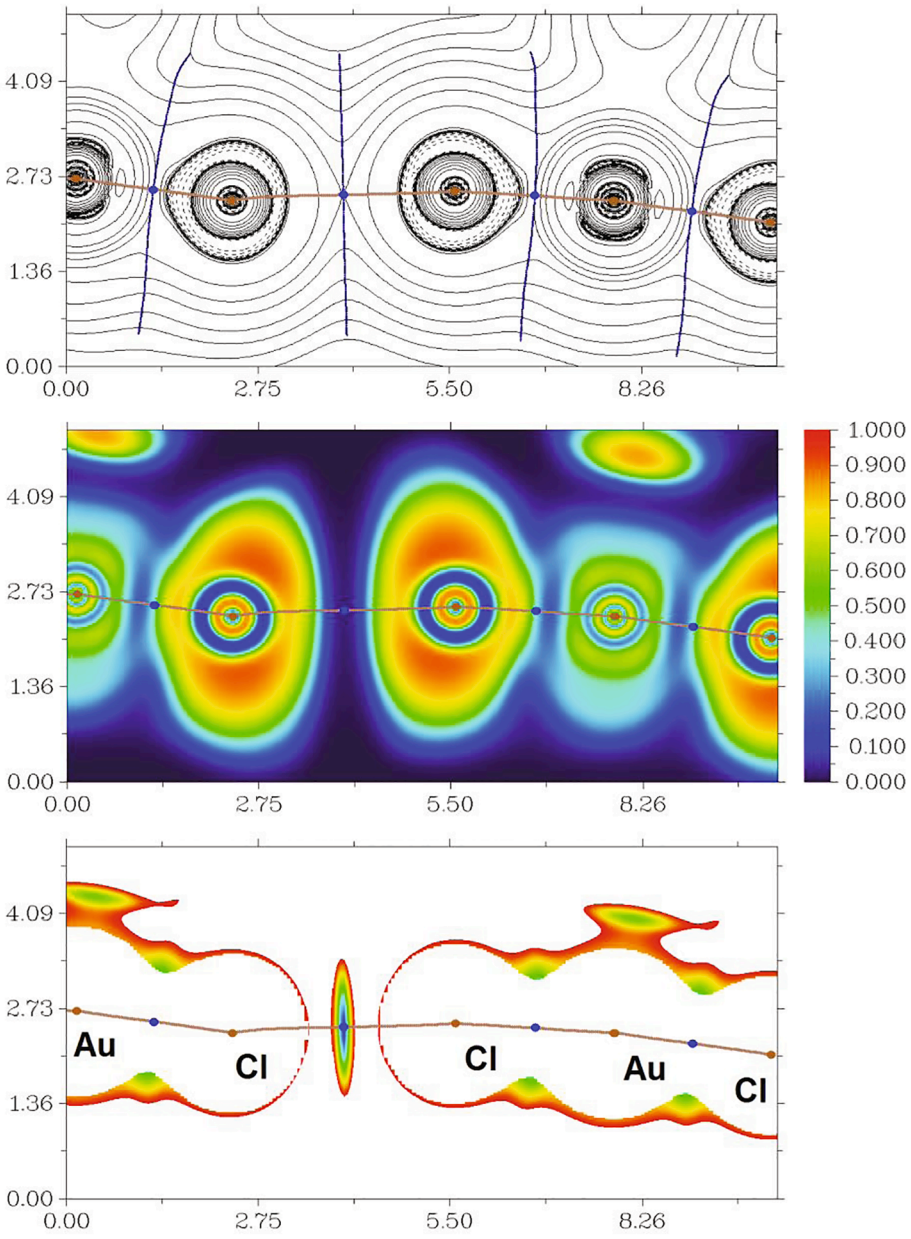

Fig. 3. Contour line diagram of the Laplacian of electron density distribution $\nabla^2\rho(\mathbf{r})$, bond paths, and selected zero-flux surfaces (top panel), visualization of electron localization function (ELF, center panel) and reduced density gradient (RDG, bottom panel) analyses for Cl···Cl noncovalent interactions in **5**. Bond critical points (3, –1) are shown in blue, nuclear critical points (3, –3) – in pale brown, bond paths are shown as pale brown lines, length units – Å, and the color scale for the ELF and RDG maps are presented in a.u.

with weakly binding to the gold(III) center azogroup.

Despite weak interaction between the azogroup and the metal center, which potentially could allow photoinduced isomerization around the N═N bond, **4** and **5** did not feature any noticeable photochromism in DCM solutions. Absorption spectra of **4** and **5** exhibited broad absorptions between 450 and 500 nm with a shoulder around 600 nm (Figs. S1 and S2), which were similar to earlier studied transition metal azoimidazole complexes. Photoluminescence (PL) spectra of **4** and **5** in CH_2Cl_2 (Fig. S3) exhibited a peak with emission maximum at 599 and 663 nm, respectively, with a moderate quantum yields (17% and 15%, respectively), while photoluminescence excitation (PLE) spectra showed peaks at 540 and 577 nm, respectively (Fig. S3). Moderate Stokes shifts (0.23 and 0.28 eV, respectively) observed between PLE and PL spectra are indicative of structural differences between the ground and excited states **4** and **5**.

Interestingly, inspection of the crystallographic data suggested the presence of interesting Cl···Cl noncovalent interactions in **5** (Fig. 2). Considering this, in addition to structural analysis, some computational study was desirable. In order to confirm or deny the hypothesis on the existence of these supramolecular contacts and quantify their energies

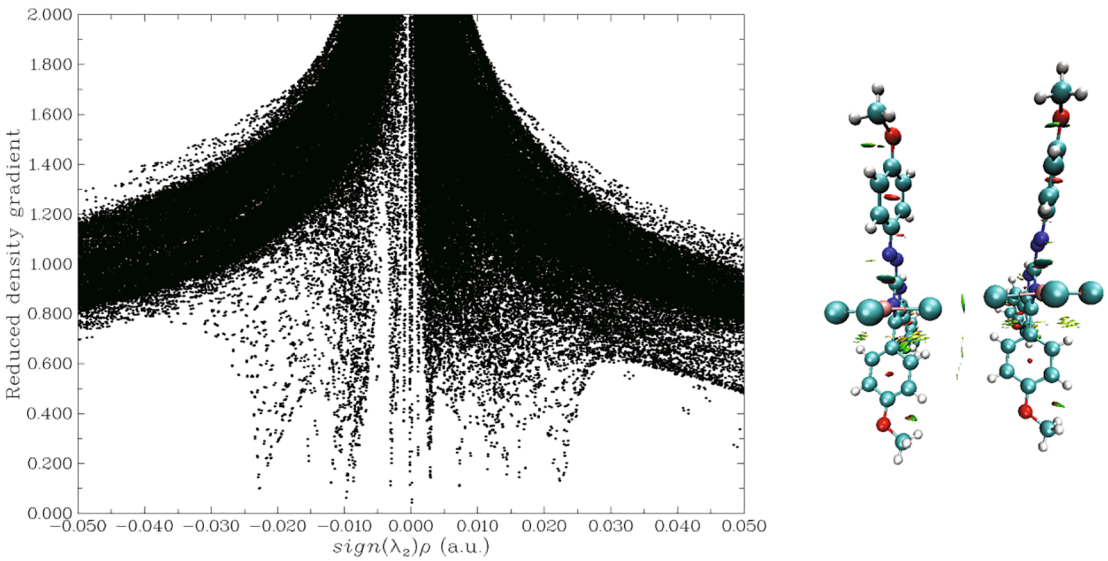

Fig. 4. NCI plot for model dimeric associate and visualization of intermolecular contacts in 3D using NCI analysis technique.

from a theoretical point of view, we carried out DFT calculations at the ωB97XD/DZP-DKH and ωB97XD/TZP-DKH levels of theory and performed topological analysis of the electron density distribution within the framework of Bader's theory (QTAIM analysis) [27] for model dimeric associate (Cartesian atomic coordinates for this model dimeric associate are presented in Supporting Information, Table S1).

Results of QTAIM analysis are summarized in Table 2, the contour line diagram of the Laplacian of electron density distribution $\nabla^2\rho(\mathbf{r})$, bond paths, and selected zero-flux surfaces, visualization of electron localization function (ELF) and reduced density gradient (RDG) analyses for Cl···Cl noncovalent interactions in **5** are shown in Fig. 3. The noncovalent interactions analysis as scatter graph of RDG vs. real space function sign(λ_2)ρ, namely the product of sign of λ_2 (second largest eigenvalue of Hessian matrix of electron density) and ρ (electron density) (NCI plot [28]) for model dimeric associate and visualization of intermolecular contacts in 3D using NCI analysis technique are shown in Fig. 4.

The shortest van der Waals radius for Cl atom is 1.75 Å [18].

[a] $E_{int} = 0.49(-V(\mathbf{r}))$ (this correlation between the interaction energy and the potential energy density of electrons at the bond critical points (3, –1) was specifically developed for noncovalent interactions involving chlorine atoms) [29].

[b] $E_{int} = 0.47G(\mathbf{r})$ (this correlation between the interaction energy and the kinetic energy density of electrons at the bond critical points (3, –1) was specifically developed for noncovalent interactions involving chlorine atoms) [29].

The QTAIM analysis demonstrates the presence of appropriate bond critical point (3, –1) for Cl···Cl contact in model dimeric associate (Table 2). The low magnitude of the electron density (0.010 a.u.), positive value of the Laplacian of electron density (0.040 a.u.), very close to zero positive energy density (0.002 a.u.) in this bond critical point (3, –1) and estimated strength for appropriate short contact (1.8–2.4 kcal/mol) are independent on the choice of basis set used for DFT calculations (double-zeta or triple-zeta quality) and typical for crystal-packing induced weak halogen···halogen noncovalent interactions with a negligible charge transfer component [22,30–32]. The balance between the Lagrangian kinetic energy G(**r**) and potential energy density V(**r**) at the bond critical point (3, –1) corresponding for Cl···Cl noncovalent interactions in **5** reveals that a covalent contribution is absent in this supramolecular contact [33]. The Laplacian of electron density is typically decomposed into the sum of contributions along the three principal axes of maximal variation, giving the three eigenvalues of the Hessian matrix (λ_1, λ_2 and λ_3), and the sign of λ_2 can be utilized to distinguish bonding

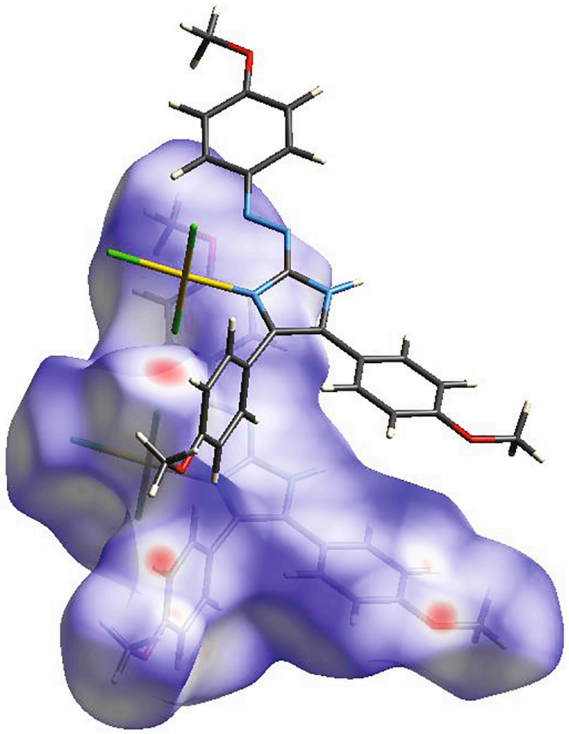

Fig. 5. Visualization of Hirshfeld surface for the X-ray structure **5**.

(attractive, $\lambda_2 < 0$) weak interactions from nonbonding ones (repulsive, $\lambda_2 > 0$) [34]. Thus, discussed Cl···Cl noncovalent interactions in **5** are attractive (Table 2).

To understand what kind of interatomic contacts give the largest contributions in crystal packing, we carried out the Hirshfeld surface analysis for the X-ray structure **5** (Fig. 5). The main partial contributions of different interatomic contacts to the Hirshfeld surface of X-ray structure **5** are: H—H 36.1%, Cl-H 22.3%, C—H 17.6%, O—H 12.1%, C—C 3.0%, N—H 2.5%, N—C 2.3%, Cl-Cl 1.2%, Au-H 1.0%, N—N 0.8%, O—C 0.7%, and Cl-C 0.3%; the contributions of other interatomic contacts are < 0.1%. Thus, the Hirshfeld surface analysis for the X-ray structure **5** reveals that crystal packing controlled primarily by interatomic contacts involving hydrogen and chlorine atoms.

Antiproliferative activity of complex **5** and cisplatin, as a control compound, was determined using a small library of human cell lines (MCF7 human breast adenocarcinoma cell line, A549 human lung carcinoma cell line, HCT116 human colon carcinoma cell line and WI38 human fibroblast-like fetal lung cell line) by means of standard MTT colorimetric assay. Complex **5** found to be significantly less active with $IC_{50} > 100$ μM (limited by solubility) compared to cisplatin (IC_{50} 12.5 ± 1.2, 12.3 ± 1.7, 8.8 ± 0.9, 3.0 ± 0.7 for MCF7, HCT116, A549 and WI38 correspondingly).

4. Conclusions

In conclusion, we synthesized first azoimidazole gold(III) complexes and characterized them using C, H, N elemental analyses, IR, UV/Vis and X-ray diffraction analysis. Interestingly, compound **5** exhibited relatively low toxicity against a library of human cell lines, which is unusual for Au(III) complexes.

Structural investigation revealed the azo group is rather weakly coordinated at the Au(III) metal center, and triarylazoimidazole trichlorogold(III) complexes could be described as square planar gold(III) complexes with weakly binding azogroup. Relatively short non-covalent chlorine···chlorine interactions (3.202 Å) were detected for **5** in the solid state and studied by DFT calculations and topological analysis of the electron density distribution within the framework of Bader's theory (QTAIM method).

CRediT authorship contribution statement

Alexander G. Tskhovrebov: Conceptualization, Methodology, Investigation, Writing - original draft, Writing - review & editing, Supervision. **Alexander S. Novikov:** Investigation, Writing - original draft, Writing - review & editing, Supervision. **Boris S. Tupertsev:** Investigation. **Alexey A. Nazarov:** Investigation. **Anastasia A. Antonets:** Investigation. **Artyom A. Astafiev:** Investigation. **Andreii S. Kritchenkov:** Investigation. **Alexey S. Kubasov:** Investigation. **Valentine G. Nenajdenko:** Investigation. **Victor N. Khrustalev:** Investigation.

Declaration of Competing Interest

The authors declare that they have no known competing financial interests or personal relationships that could have appeared to influence the work reported in this paper.

Acknowledgement

This paper has been supported by the Ministry of Education and Science of the Russian Federation (award no. 075-03-2020-223 (FSSF-2020-0017)) and the RUDN University Strategic Academic Leadership Program. Funding for this research was provided by Russian Foundation for Basic Research (project number 20-53-00006) and Belarusian Foundation for Fundamental Research (grant X20P-066).

Appendix A. Supplementary data

Supplementary data to this article can be found online at https://doi.org/10.1016/j.ica.2021.120373.

References

[1] A.G. Tskhovrebov, L.C.E. Naested, E. Solari, R. Scopelliti, K. Severin, Synthesis of azoimidazolium dyes with nitrous oxide, Angew. Chemie - Int. Ed. 54 (4) (2015) 1289–1292, https://doi.org/10.1002/anie.201410067.

[2] J. Otsuki, K. Suwa, K.K. Sarker, C. Sinha, Photoisomerization and thermal isomerization of arylazoimidazoles, J. Phys. Chem. A 111 (8) (2007) 1403–1409, https://doi.org/10.1021/jp066816p10.1021/jp066816p.s001.

[3] S. Crespi, N.A. Simeth, B. König, Heteroaryl azo dyes as molecular photoswitches, Nat. Rev. Chem. 3 (3) (2019) 133–146, https://doi.org/10.1038/s41570-019-0074-6.

[4] A. Presa, R.F. Brissos, A.B. Caballero, I. Borilovic, L. Korrodi-Gregório, R. Pérez-Tomás, O. Roubeau, P. Gamez, Photoswitching the cytotoxic properties of platinum (II) compounds, Angew. Chemie - Int. Ed. (2015), https://doi.org/10.1002/anie.201412157.

[5] K.K. Sarker, B.G. Chand, K. Suwa, J. Cheng, T.-H. Lu, J. Otsuki, C. Sinha, Structural studies and photochromism of mercury(II)-iodo complexes of (arylazo)imidazoles, Inorg. Chem. 46 (3) (2007) 670–680, https://doi.org/10.1021/ic061221u10.1021/ic061221u.s00110.1021/ic061221u.s002.

[6] K.K. Sarker, D. Sardar, K. Suwa, J. Otsuki, C. Sinha, Cadmium(II) complexes of (Arylazo)imidazoles: synthesis, structure, photochromism, and density functional theory calculation, Inorg. Chem. 46 (2007) 8291–8301, https://doi.org/10.1021/ic7012073.

[7] C. Schütt, G. Heitmann, T. Wendler, B. Krahwinkel, R. Herges, Design and synthesis of photodissociable ligands based on azoimidazoles for light-driven coordination-induced spin state switching in homogeneous solution, J. Org. Chem. 81 (3) (2016) 1206–1215, https://doi.org/10.1021/acs.joc.5b0281710.1021/acs.joc.5b02817.s001.

[8] D. Das, M.K. Nayak, C. Sinha, Chemistry of azoimidazoles. Synthesis, spectral characterization and redox studies of N(1)-benzyl-2-(arylazo)imidazolepalladium (II)chloride, Transit. Met. Chem. 22 (1997) 172–175, https://doi.org/10.1023/A:1018427432703.

[9] T.K. Misra, D. Das, C. Sinha, Chemistry of azoimidazoles: synthesis, spectral characterization and redox properties of bis(N(1)-alkyl-2-(arylazo)imidazole) copper(I) and silver(I) complexes, Polyhedron 16 (1997) 4163–4170, https://doi.org/10.1016/S0277-5387(97)00127-7.

[10] A. Chawla, V. Kapoor, Microwave assisted synthesis of 2-amino-3,4,5-trisubstituted imidazolines using radiszewski method, their characterisation and evaluation for antioxidant activity, Int. Res. J. Pharm. (2016), https://doi.org/10.7897/2230-8407.0711123.

[11] J.-D. Chai, M. Head-Gordon, Long-range corrected hybrid density functionals with damped atom–atom dispersion corrections, Phys. Chem. Chem. Phys. 10 (2008) 6615–6620, https://doi.org/10.1039/B810189B.

[12] C.L. Barros, P.J.P. de Oliveira, F.E. Jorge, A. Canal Neto, M. Campos, Gaussian basis set of double zeta quality for atoms Rb through Xe: application in non-relativistic and relativistic calculations of atomic and molecular properties, Mol. Phys. 108 (2010) 1965–1972. 10.1080/00268976.2010.499377.

[13] A. Canal Neto, F.E. Jorge, All-electron double zeta basis sets for the most fifth-row atoms: application in DFT spectroscopic constant calculations, Chem. Phys. Lett. 582 (2013) 158–162, https://doi.org/10.1016/j.cplett.2013.07.045.

[14] T. Lu, F. Chen, Multiwfn: a multifunctional wavefunction analyzer, J. Comput. Chem. 33 (2012) 580–592, https://doi.org/10.1002/jcc.22885.

[15] W. Humphrey, A. Dalke, K. Schulten, VMD: visual molecular dynamics, J. Mol. Graph. 14 (1996) 33–38, https://doi.org/10.1016/0263-7855(96)00018-5.

[16] M.A. Spackman, D. Jayatilaka, Hirshfeld surface analysis, CrystEngComm 11 (1) (2009) 19–32, https://doi.org/10.1039/B818330A.

[17] J.J. McKinnon, D. Jayatilaka, M.A. Spackman, Towards quantitative analysis of intermolecular interactions with Hirshfeld surfaces, Chem. Commun. (2007) 3814–3816, https://doi.org/10.1039/b704980c.

[18] A. Bondi, Van der Waals volumes and radii of metals in covalent compounds, J. Phys. Chem. 70 (9) (1966) 3006–3007, https://doi.org/10.1021/j100881a503.

[19] A.G. Tskhovrebov, E. Solari, R. Scopelliti, K. Severin, Reactions of grignard reagents with nitrous oxide, Organometallics 33 (10) (2014) 2405–2408, https://doi.org/10.1021/om500333y.

[20] Y. Liu, P. Varava, A. Fabrizio, L.Y.M. Eymann, A.G. Tskhovrebov, O.M. Planes, E. Solari, F. Fadaei-Tirani, R. Scopelliti, A. Sienkiewicz, C. Corminboeuf, K. Severin, Synthesis of aminyl biradicals by base-induced Csp3–Csp3 coupling of cationic azo dyes, Chem. Sci. 10 (22) (2019) 5719–5724, https://doi.org/10.1039/C9SC01502G.

[21] L.Y.M. Eymann, A.G. Tskhovrebov, A. Sienkiewicz, J.L. Bila, I. Živković, H. M. Rønnow, M.D. Wodrich, L. Vannay, C. Corminboeuf, P. Pattison, E. Solari, R. Scopelliti, K. Severin, Neutral aminyl radicals derived from azoimidazolium dyes, J. Am. Chem. Soc. 138 (46) (2016) 15126–15129, https://doi.org/10.1021/jacs.6b0912410.1021/jacs.6b09124.s00110.1021/jacs.6b09124.s00210.1021/jacs.6b09124.s00310.1021/jacs.6b09124.s00410.1021/jacs.6b09124.s00510.1021/jacs.6b09124.s006.

[22] V.G. Nenajdenko, N.G. Shikhaliyev, A.M. Maharramov, K.N. Bagirova, G. T. Suleymanova, A.S. Novikov, V.N. Khrustalev, A.G. Tskhovrebov, Halogenated diazabutadiene dyes: synthesis, structures, supramolecular features, and theoretical studies, Molecules 25 (2020) 5013, https://doi.org/10.3390/molecules25215013.

[23] A.G. Tskhovrebov, J.B. Lingnau, A. Fürstner, Gold difluorocarbenoid complexes: spectroscopic and chemical profiling, Angew. Chemie - Int. Ed. 58 (26) (2019) 8834–8838, https://doi.org/10.1002/anie.v58.2610.1002/anie.201903957.

[24] A.G. Tskhovrebov, R. Goddard, A. Fürstner, Two amphoteric silver carbene clusters, Angew. Chemie - Int. Ed. 57 (27) (2018) 8089–8094, https://doi.org/10.1002/anie.v57.2710.1002/anie.201803246.

[25] V.N. Mikhaylov, V.N. Sorokoumov, D.M. Liakhov, A.G. Tskhovrebov, I.A. Balova, Polystyrene-supported acyclic diaminocarbene palladium complexes in Sonogashira cross-coupling: stability vs. catalytic activity, Catalysts 8 (2018) 141, https://doi.org/10.3390/catal8040141.

[26] A.G. Tskhovrebov, K.V. Luzyanin, M. Haukka, V.Y. Kukushkin, Synthesis and characterization of cis-(RNC)2PtII species useful as synthons for generation of

various (aminocarbene)Pt II complexes, J. Chem. Crystallogr. 42 (12) (2012) 1170–1175, https://doi.org/10.1007/s10870-012-0371-0.
[27] R.F.W. Bader, A quantum theory of molecular structure and its applications, Chem. Rev. 91 (5) (1991) 893–928, https://doi.org/10.1021/cr00005a013.
[28] E.R. Johnson, S. Keinan, P. Mori-Sánchez, J. Contreras-García, A.J. Cohen, W. Yang, Revealing noncovalent interactions, J. Am. Chem. Soc. 132 (18) (2010) 6498–6506, https://doi.org/10.1021/ja100936w.
[29] E.V. Bartashevich, V.G. Tsirelson, Interplay between non-covalent interactions in complexes and crystals with halogen bonds, Russ. Chem. Rev. 83 (12) (2014) 1181–1203, https://doi.org/10.1070/RCR4440.
[30] S.A. Adonin, M.A. Bondarenko, A.S. Novikov, P.A. Abramov, M.N. Sokolov, V. P. Fedin, Halogen bonding in the structures of pentaiodobenzoic acid and its salts, CrystEngComm 21 (43) (2019) 6666–6670, https://doi.org/10.1039/C9CE01106D.
[31] A.N. Usoltsev, S.A. Adonin, A.S. Novikov, D.G. Samsonenko, M.N. Sokolov, V. P. Fedin, One-dimensional polymeric polybromotellurates(IV): Structural and theoretical insights into halogen···halogen contacts, CrystEngComm 19 (2017) 5934–5939, https://doi.org/10.1039/c7ce01487b.
[32] A.G. Tskhovrebov, A.S. Novikov, A.S. Kritchenkov, V.N. Khrustalev, M. Haukka, Attractive halogen···halogen interactions in crystal structure of trans-dibromogold (III) complex, Zeitschrift Fur Krist. - Cryst. Mater. 25 (2020) 477–480, https://doi.org/10.1515/zkri-2020-0045.
[33] E. Espinosa, I. Alkorta, J. Elguero, E. Molins, From weak to strong interactions: A comprehensive analysis of the topological and energetic properties of the electron density distribution involving X-H···F-Y systems, J. Chem. Phys. 117 (2002) 5529–5542, https://doi.org/10.1063/1.1501133.
[34] J. Contreras-García, E.R. Johnson, S. Keinan, R. Chaudret, J.-P. Piquemal, D. N. Beratan, W. Yang, NCIPLOT: a program for plotting noncovalent interaction regions, J. Chem. Theory Comput. 7 (2011) 625–632, https://doi.org/10.1021/ct100641a.